

Testing Cosmology with Cosmic Sound Waves

Pier Stefano Corasaniti¹ and Alessandro Melchiorri^{2,3}

¹*LUTH, Observatoire de Paris, CNRS UMR 8102, Université Paris Diderot,
5 Place Jules Janssen, 92195 Meudon Cedex, France*

²*Dipartimento di Fisica e Sezione INFN, Università degli Studi di Roma “La Sapienza”, Ple Aldo Moro 5, 00185, Rome, Italy*

³*CERN, Theory Division, CH-1211 Geneva 23, Switzerland*

(Dated: May 18, 2019)

WMAP observations have accurately determined the position of the first two peaks and dips in the CMB temperature power spectrum. These encode information on the ratio of the distance to the last scattering surface to the sound horizon at decoupling. However pre-recombination processes can contaminate this distance information. In order to assess the amplitude of these effects we use the WMAP data and evaluate the relative differences of the CMB peaks and dips multipoles. We find that the position of the first peak is largely displaced with the respect to the expected position of the sound horizon scale at decoupling. In contrast the relative spacings of the higher extrema are statistically consistent with those expected from perfect harmonic oscillations. This provides evidence for a scale dependent phase shift of the CMB oscillations which is caused by gravitational driving forces affecting the propagation of sound waves before recombination. By accounting for these effects we have performed a MCMC likelihood analysis of the location of WMAP extrema to constrain in combination with recent BAO data a constant dark energy equation of state parameter w . For a flat universe we find a strong 2σ upper limit $w < -1.10$, and including the HST prior we obtain $w < -1.14$. On the other hand we infer larger limits for non-flat cosmologies. From the full CMB likelihood analysis we also estimate the values of the shift parameter R and the multipole l_a of the acoustic horizon at decoupling for several cosmologies to test their dependence on model assumptions. Although the analysis of the full CMB spectra should be always preferred, using the position of the CMB peaks and dips provide a simple and consistent method for combining CMB constraints with other datasets.

Keywords: cosmology: observations — CMB

I. INTRODUCTION

Cosmic Microwave Background (CMB) observations have provided crucial insights into the origin and evolution of present structures in the universe [1, 2, 3]. Physical processes occurred before, during and after recombination have left distinctive signatures on the CMB. The most prominent feature is a sequence of peaks and dips in the anisotropy power spectrum, the remnant imprints of acoustic waves propagating in the primordial photon-baryon plasma at the time of decoupling [4, 5, 6]. This oscillatory pattern carries specific information on several cosmological parameters [7]. As an example the angular scale at which these oscillations are observed provides a distance measurement of the last scattering surface to the sound horizon at decoupling, hence a clean test of cosmic curvature [8].

WMAP observations have accurately detected the peak structure of the CMB power spectrum. These data have constrained the geometry of the universe to be nearly flat and have precisely determined other cosmological parameters [9]. On the other hand constraints on dark energy are less stringent, this is because its late time effects leave a weaker imprint of the CMB which is diluted by degeneracies with other parameters. Indeed other cosmological tests can be more sensitive to the signature of dark energy, nonetheless they still require additional information from CMB to break the parameter degeneracies. As an example CMB constraints are usu-

ally combined with those from SN Ia luminosity distance data. Alternatively the CMB can be used in combination with measurements of the baryon acoustic oscillations (BAO) in the galaxy power spectrum [10]. In fact the same acoustic signature present in the CMB is also imprinted in the large scale distribution of galaxy, thus providing a complementary probe of cosmic distances at lower redshifts.

A likelihood analysis of the CMB spectra is certainly the more robust approach to implement CMB constraints with those from other datasets. This can be very time consuming, henceforth one can try to compress the CMB information in few measurable and easily computable quantities. Recent literature has focused on the use of the shift parameter R , and the multipole of the acoustic scale at decoupling l_a [11, 12]. However these quantities are not directly measured by CMB observations, they are inferred as secondary parameters from the cosmological constraints obtained from the full CMB likelihood analysis. Consequently their use as *data* can potentially lead to results which suffer of model dependencies as well as prior parameter assumptions made in the analysis from which the values of R (l_a) have been inferred in the first place. In contrast the multipole location of the CMB extrema can be directly determined from the observed temperature power spectrum through model-independent curve fitting. These measurements can then be used to constrain cosmological parameters provide that pre-recombination corrections are properly taken into account.

In this paper we analyse in detail the cosmological information encoded in the position of the CMB extrema as measured by WMAP. Our aim is to provide a simple and unbiased method for incorporating CMB constraints into other datasets which is alternative to that of using R and/or l_a [11, 12]. Firstly we estimate the amplitude of pre-recombination mechanisms that can displace the location of the CMB extrema with the respect to the angular scale of the sound horizon at decoupling. In particular we show that the WMAP location of the first peak is strongly affected by such mechanisms, while the displacements induced on the higher peaks and dips are smaller. By accounting for these effects we perform a cosmological parameter analysis and infer constraints on dark energy under different prior assumptions, including the cosmic curvature. We then combine these results with measurements of BAO from SDSS and 2dF data [13]. Finally we test for potential model dependencies of R (and l_a) by performing a full likelihood analysis of the WMAP spectra for different sets of cosmological parameters.

The paper is organized as follows: in Section II we review the physics of the CMB acoustic oscillations. In Section III we discuss the relative shifts of the multipoles of the WMAP peaks and dips. In Section IV we present the results of the cosmological parameter inference using the location of the CMB extrema in combination with BAO. We discuss the results on the shift parameter in Section V and present our conclusions in Section VI.

II. CMB ACOUSTIC OSCILLATIONS

The onset of acoustic waves on the sub-horizon scales of the tightly coupled photon-baryon plasma before recombination is natural consequence of photon pressure resisting gravitational collapse. The properties of these oscillations depends both on the background expansion and the evolution of the gravitational potentials associated with the perturbations present in the system. In the following we will briefly review the basic processes which affect the propagation of these waves before decoupling. Interested readers will find more detailed discussions in [6, 7]. Let consider the photon temperature fluctuation $\Theta_0 \equiv \Delta T$ (monopole), following Hu and Sugiyama [6] its evolution is described by

$$\ddot{\Theta}_0 + \frac{\dot{R}}{1+R}\dot{\Theta}_0 + k^2 c_s^2 \Theta_0 = F(\eta), \quad (1)$$

where the dot is the derivative with respect to conformal time, $R = 3\rho_b/4\rho_\gamma$ is the baryon-to-photon ratio, k is the wavenumber, $c_s = c/\sqrt{3(1+R)}$ is the sound speed of the system with c the speed of light. The source term

$$F = -\ddot{\Phi} - \frac{\dot{R}}{1+R}\dot{\Phi} - k^2 \frac{\Psi}{3}, \quad (2)$$

represents a driving force, where Φ and Ψ are the gauge-invariant metric perturbations respectively.

It is easy to see from Eq. (1) that the homogeneous equation ($F = 0$) admits oscillating solutions of the form,

$$\Theta_0^{\text{hom}}(\eta) = A_1 \cos kr_s(\eta) + \frac{A_2}{k} \sin kr_s(\eta) \quad (3)$$

where A_1 and A_2 are set by the initial conditions and $r_s(\eta) = \int_0^\eta c_s(\eta') d\eta'$ is the sound horizon at time η . At time of decoupling η_* , the positive and negative extrema of these oscillations appear as a series of peaks in the anisotropy power spectrum. Their location in the multipole space is a multiple integer of the inverse of the angle subtended by the sound horizon scale at decoupling, namely $l_m^{\text{peak}} = m l_a$ with $m = 1, 2, \dots$ and

$$l_a = \pi \frac{r_K(z_*)}{r_s(z_*)}, \quad (4)$$

where z_* is the recombination redshift and $r(z)$ the co-moving distance to z ,

$$r_K(z) = \frac{c}{H_0} \frac{1}{\sqrt{|\Omega_K|}} f(\sqrt{|\Omega_K|} I(z)), \quad (5)$$

with H_0 the Hubble constant, $|\Omega_K| = -K/H_0^2$ with K the constant curvature, $f(x) = \sin(x), \sinh(x), x$ for $K > 0, < 0$ and $= 0$ respectively, and $I(z) = \int_0^z dz' H_0/H(z')$.

Scales for which the monopole vanishes also contribute to anisotropy power spectrum. In such a case the signal comes from the non-vanishing photon velocity Θ_1 (dipole) which oscillates with a phase shifted by $\pi/2$ with the respect to the monopole [6]. Therefore photons coming from these regions are responsible for a series of troughs in the anisotropy power spectrum at multipoles $l_n^{\text{dip}} = n l_a$ with $n = m + 1/2$.

The full solution to Eq. (1) at decoupling reads as [14]:

$$\Theta_0(\eta_*) = \Theta_0^{\text{hom}}(\eta_*) + \frac{A_3}{k} \int_0^{\eta_*} d\eta' [1 + R(\eta')]^{3/4} \sin[kr_s(\eta_*) - kr_s(\eta')] F(\eta'), \quad (6)$$

where A_3 is set by the initial conditions. As we can see from Eq. (6) including the driving force F induces a scale

dependent phase shift of the acoustic oscillations, which is primarily caused by the time variation of the gravita-

tional potential Φ . In fact perturbations on scales which enter the horizon at the matter-radiation equality experience a variation of the expansion rate which causes a time evolution of the associated gravitational potentials. This mechanism is dominant on the large scales and is responsible for the so called early Integrated Sachs-Wolfe (ISW) effect [15]. The overall effect is to displace the acoustic oscillations with the respect to the pure harmonic series. For a spectrum of adiabatic perturbations we may expect this displacement to become negligible on higher harmonics since the gravitational potentials decay as $\Phi \propto (k\eta)^{-2}$ on scales well inside the horizon. This is not the case if active perturbations were present on such scales before the epoch of decoupling.

In order to account for these pre-recombination effects a realistic modeling of the multipole position of the CMB maxima and minima is given by [16]

$$l_m = l_a(m - \varphi_m), \quad (7)$$

where $m = 1, 2, \dots$ for peaks, and $m = 3/2, 5/2, \dots$ for dips; φ_m parametrizes the displacement caused by the driving force. Because of the scale dependent nature of the driving effect discussed above, it is convenient to decompose the correction term as $\varphi_m = \bar{\varphi} + \delta\varphi_m$, where $\bar{\varphi} \equiv \varphi_1$ is the overall shift of the first peak with respect to the sound horizon, and $\delta\varphi_m$ is the shift of the m -th extrema relative to the first peak [17].

It is worth noticing that while the position of the CMB extrema depends through l_a on the geometry and late time expansion of the universe, their relative spacing depends through φ_m only on pre-recombination physics.

III. PHASE SHIFT OF WMAP PEAKS AND DIPS

WMAP observations have provided an accurate determination of the CMB power spectrum. The multipoles of the CMB extrema have been inferred using a functional fit to the uncorrelated band powers as described in [18]. Hinshaw et al. [3] have applied this method to the WMAP-3yr data and found the position of the first two peaks and dips to be at $l_1 = 220.8 \pm 0.7$, $l_{3/2} = 412.4 \pm 1.9$, $l_2 = 530.9 \pm 3.8$ and $l_{5/2} = 675.2 \pm 11.1$ respectively.

We want to determine whether these measurements provide any evidence for driving effects affecting the acoustic oscillations. In order to do so we evaluate the relative spacings between the WMAP measured m -th and m' -th extrema,

$$\Delta_{m,m'} = \frac{l_{m'}}{l_m} - 1, \quad (8)$$

and the propagated errors $\sigma_{\Delta_{m,m'}}$.

Let first consider the spacings relative to the location of the first peak. We find $\Delta_{1,3/2} = 0.87 \pm 0.01$, $\Delta_{1,2} = 1.40 \pm 0.02$ and $\Delta_{1,5/2} = 2.06 \pm 0.05$ respectively. These estimates are shown in Figure 1 (black solid circles), where we also plot the relative spacings as expected

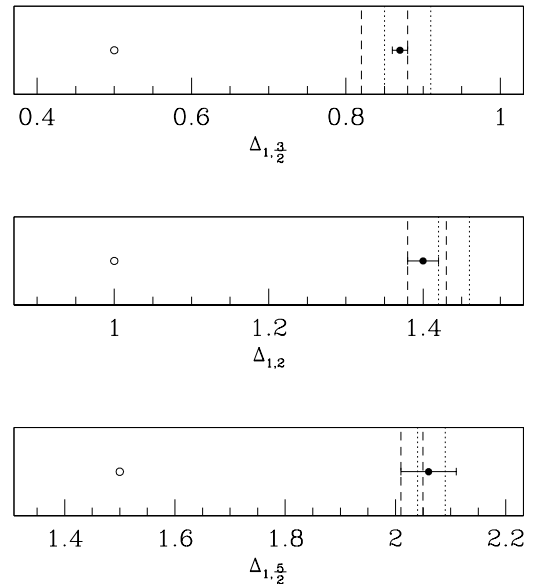


FIG. 1: WMAP spacings of $l_{3/2}$, l_2 and $l_{5/2}$ relative to l_1 (black solid circles) and propagated errors. The values expected from the harmonic series are $\Delta_{1,3/2} = 1/2$, $\Delta_{1,2} = 1$ and $\Delta_{1,5/2} = 3/2$ (open circles). Vertical dashed lines delimit the expected interval of variation of the relative spacings obtained by including the shift corrections as parametrized in [17] and evaluated over a conservative range of cosmological parameter values (see text). The dotted vertical lines include the effect of three massless neutrinos.

from a sequence of perfect acoustic oscillations (open circles). It is evident that the WMAP inferred values of $\Delta_{1,m}$ lie many sigmas away from those expected from the harmonic series. This provides clear evidence that the position of the first peak is largely affected by the driving force at decoupling. Such a large displacement is most likely caused by the early ISW, although an additional contribution from isocurvature fluctuations [19] or active gravitational potentials [20] cannot be excluded.

Let focus now on the displacement of the second peak relative to the first one, since $\Delta_{1,2} > 1$ it follows that $\bar{\varphi} > \delta\varphi_2$. This implies that the overall shift of l_1 with the respect to l_a is larger than the shift of l_2 relative to l_1 . As discussed in the previous section this is consistent with having the gravitational potentials inside the sound horizon scaling as $\Phi \propto (k\eta)^{-2}$, thus inducing a weaker driving force. This can be seen more clearly in Figure 2 where we plot $\Delta_{3/2,2}$, $\Delta_{2,5/2}$ and $\Delta_{3/2,5/2}$.

Apart $\Delta_{2,3/2} = 0.29 \pm 0.01$, whose value suggests the presence of a non-negligible driving effect still on the scale of the first dip, we may notice that all other spacings are statistically consistent with the prediction of the harmonic series.

Therefore these results suggest the existence of a scale dependent phase shift of the CMB acoustic oscillations. The effect is larger on the scale of the first acoustic peak,

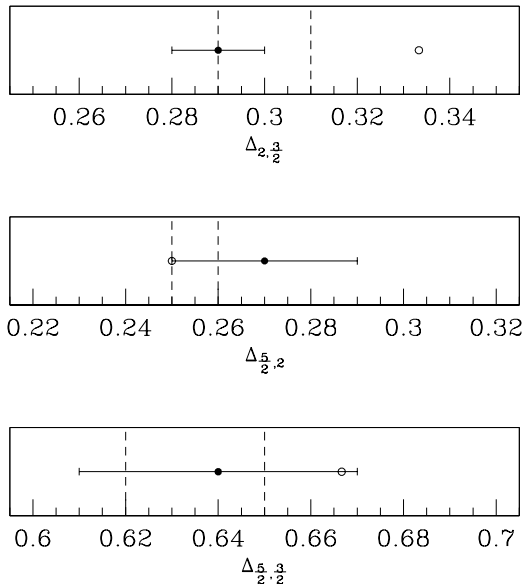


FIG. 2: As in Figure 1 for $l_{3/2}$, l_2 and $l_{5/2}$ relative spacings. The harmonic series values are $\Delta_{3/2,2} = 1/3$, $\Delta_{2,5/2} = 1/4$ and $\Delta_{3/2,5/2} = 2/3$.

while it is weaker for the higher harmonics. The upcoming Planck mission will map more accurately the location of the higher peaks and dips and provide a cleaner detection of this shift.

Indeed driving effects are well accounted for by the CMB theory as incorporated in standard Boltzmann codes [21]. For instance a standard adiabatic spectrum of initial density perturbations leads to phase shifts which are consistent with those we have inferred here. To show this we have used the fitting formulas provided in [17] for adiabatic models which parametrize φ_m in terms of the total matter density $\Omega_m h^2$, the baryon density $\Omega_b h^2$, the dark energy density at decoupling Ω_{DE}^{dec} and the scalar spectral index n_s . Assuming $\Omega_{DE}^{dec} = 0$ we evaluate these formulas over the following range of parameter values, $0.08 < \Omega_m h^2 < 0.11$, $0.020 < \Omega_b h^2 < 0.024$, $0.92 < n_s < 1.1$ and infer the corresponding intervals for the relative spacings $\Delta_{m,m'}$. These are drawn in Figure 1 and 2 as vertical dashed lines. It can be seen that these intervals are statistically consistent with the measured spacings. Including the contribution of three massless neutrinos (dotted vertical lines) slightly shifts the $\Delta_{1,m}$ intervals further from the expected values of the perfect harmonic oscillator. This is because the presence of relativistic neutrinos extend the radiation era and therefore leads to a more effective early ISW effect on the large scales. In contrast we find no differences for the intervals of the other peaks and dips spacings.

IV. PARAMETER INFERENCE

We perform a Markov Chain Monte Carlo (MCMC) likelihood analysis to derive cosmological parameter constraints using the measurements of the WMAP extrema discussed in the previous section. Again we account for the shift corrections by evaluating the model prediction for l_m using Eq. (7), with the displacements φ_m parametrized as in [17]. We compute the recombination redshift z_* using the fitting formulae provided in [22]. Cosmological constraints derived from the location of the CMB peaks have been presented in previous works (e.g. [23, 24, 25]). Here our aim is to derive bounds on dark energy which are independent of Supernova Ia data and rely only on the cosmic distance information encoded in the angular scale of the sound horizon as inferred from the multipole position of the WMAP peaks and dips, and BAO measurements.

First we consider flat models with dark energy parametrized by a constant equation of state w . We then test the stability of the inferred constraints by extending the analysis to models with non-vanishing curvature, $\Omega_k \neq 0$. We also consider flat dark energy models with a time varying equation of state parametrized as $w = w_0 + w_1(1 - a)$ (CPL) [26, 27]. The credible intervals on the parameters of interest are inferred after marginalizing over h , $\Omega_b h^2$ and n_s respectively. We let them vary in the following intervals: $0.40 < h < 1.00$, $0.020 < \Omega_b h^2 < 0.024$ and $0.94 < n_s < 1.10$. Marginalizing over these parameters is necessary due to the parameter degeneracies in r_K , r_s and to properly account for the shift corrections φ_m .

As complementary dataset we use the cosmic distance as inferred from the BAO in the SDSS and 2dF surveys [13]. These measurements consists of the ratio $r_s(z_*)/D_V(z)$, where $D_V(z)$ is a distance measure given by

$$D_V(z) = [(1+z)^2 D_A(z) cz / H(z)]^{1/3}, \quad (9)$$

with $D_A(z) = r_K(z)/(1+z)$ the angular diameter distance at z . In particular Percival et al. [13] have found, $D_V(0.35)/D_V(0.2) = 1.812 \pm 0.060$.

In order to reduce the degeneracy with the Hubble parameter we also infer constraints assuming a Gaussian HST prior $h = 0.72 \pm 0.08$ [28]. In Figure 3 we plot the marginalized 1 and 2σ contours in the $\Omega_m - w$, $w - \Omega_K$ and $w_0 - w_1$ respectively. The upper panels correspond to constraints inferred from WMAP extrema alone, while the lower panels include the BAO data. Dashed contours are inferred under the HST prior. To be conservative we only quote marginalized 2σ limits. We now discuss these results in more detail.

A. Limits from CMB peaks and dips

As it can be seen in Figure 3 (upper left panel) the CMB extrema alone poorly constrain the $\Omega_m - w$ plane.

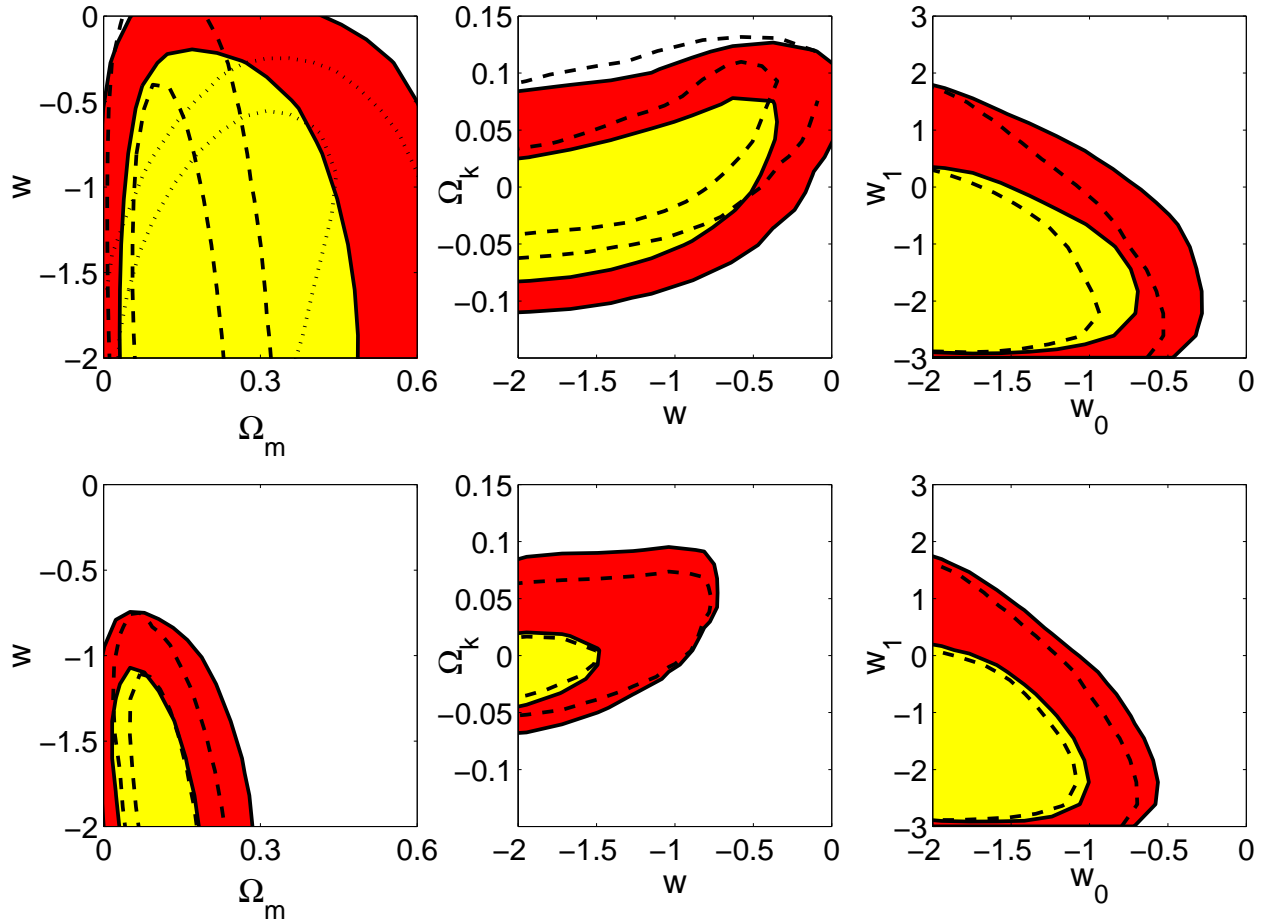


FIG. 3: Marginalized 1 and 2σ likelihood contours from WMAP extrema (upper panels) and in combination with BAO (lower panels). Dashed lines correspond to contours inferred under HST prior. The dotted lines in the upper left panel correspond to limits inferred assuming $\Omega_b h^2 = 0.023$ and $n_s = 0.96$.

In particular the 1 and 2σ regions are larger than those obtained from the WMAP analysis [9]. This is because due to the late ISW effect more information about dark energy is contained in the full CMB spectrum than just in the distance to the last scattering surface as encoded in the position of the CMB peaks and dips. A direct consequence of this is that our limits on w are unbounded from below. After marginalizing over all parameters we find $\Omega_m = 0.29 \pm_{0.23}^{0.41}$ and $w < -0.18$ at 2σ . A model with $\Omega_m = 1$ is consistent at 95% confidence level with the location of the WMAP extrema provided that $h \approx 0.42$. This is in agreement with the results presented in [29]. On the other hand imposing an HST prior (dash contours) reduce the degeneracy in the Ω_m - w plane, and the marginalized 2σ limits are $\Omega_m = 0.16 \pm_{0.11}^{0.15}$ and $w < -0.25$ respectively. The upper limit on w improves if a strong prior on $\Omega_b h^2$ and n_s is assumed (dotted contours in the upper left panel). As an example imposing $\Omega_b h^2 = 0.0223$ and $n_s = 0.96$, we find $w < -0.65$ at 2σ .

How much these bounds depend on the flatness assumption? As shown in Fig. 3 (central upper panel) extending the analysis to non-flat models increases the

geometric degeneracy and consequently leads to larger uncertainties in w . For instance the 2σ marginalized constraints are $w < -0.34$ and $\Omega_K = -0.01 \pm 0.05$ respectively, and do not improve significantly under the HST prior.

The position of the CMB peaks and dips alone does not provide any insight on the time variation of dark energy. As it can be seen in Fig. 3 (right upper panel) the contours in the w_0 - w_1 plane are spread over a large range of values. After marginalizing we find $w_0 < -0.55$ and $w_1 < 1.68$ at 2σ .

B. Combined constraints from CMB extrema and BAO

The baryon acoustic oscillations in the galaxy power spectrum provide a cosmic distance test at low redshifts. Therefore in combination with CMB measurements they can significantly reduce the cosmological parameter degeneracies. In Fig. 3 (lower left panel) we plot the combined 1 and 2σ contours in the Ω_m - w plane. At 95%

confidence level we find $\Omega_m = 0.12 \pm 0.12$ and $w < -1.10$ respectively. Imposing the HST prior further constraints the dark energy equation of state, $w < -1.14$. These results are compatible with those found in [13]. A model with $\Omega_m = 1$ is now excluded with high confidence level since the combination of CMB extrema and BAO constrain the Hubble parameter in the range $h = 0.71 \pm 0.20$ at 2σ (see also [29]). Interestingly the Λ CDM case ($w = -1$) appears to be on the edge of the 2σ limit, hence favoring non-standard dark energy models. Indeed unaccounted systematics effects in the BAO data can be responsible for such super-negative values of w . On the other hand if confirmed this would provide evidence for an exotic phantom dark energy component [30] or interpreted as the cosmological signature of a dark sector interactions (e.g. [31]).

The credible regions for non-flat models are shown in Fig. 3 (central lower panel). In this case we find $\Omega_K = -0.011 \pm 0.064$ and $w < -0.46$ at 2σ . These bounds do not change significantly under the HST prior. In Fig. 3 (lower right panel) we plot the 1 and 2σ contours in the w_0 - w_1 plane. Also in this case the bounds on a time varying dark energy equation of state remain large. For instance we find the marginalized 2σ limits to be $w_0 < -0.74$ and $w_1 < 1.6$. Necessarily inferring tighter bounds on w_1 will require the combination of several other datasets such as SN Ia luminosity distance measurements [32].

V. SHIFT PARAMETER

The geometric degeneracy of the CMB power spectrum implies that different cosmological models will have similar spectra if they have nearly identical matter densities $\Omega_m h^2$ and $\Omega_b h^2$, primordial spectrum of fluctuations and shift parameter $R = \sqrt{\Omega_m H_0^2 r_K(z_*)}$ [33]. The authors of [12] have suggested that since l_a is nearly uncorrelated with R , then both parameters can be used to further compress CMB information and combined with other measurements in a friendly user manner. For minimal extension of the dark energy parameters the inferred values of R and l_a do not significantly differ from those inferred assuming the vanilla Λ CDM model [11, 12]. Indeed differences may arise if additional parameters, such as the neutrino mass, the running of the scalar spectral index or tensor modes are considered [11]. We extend this analysis to other models. In particular by running a MCMC likelihood analysis of the full WMAP-3yrs spectra we infer constraints on R and l_a for models with an extra-background of relativistic particles (characterized by the number of relativistic species $N_{eff} \neq 3$) [34], neutrino mass [35], a time varying equation of state parametrized in the form of CPL, and a dark energy component with perturbations characterized by the sound speed c_{de}^2 . We also consider models with a running of the scalar spectral index, with a non-vanishing tensor contribution (see e.g. [36]) and, finally, with extra-features in the primordial

Model	R	l_a
Λ CDM	1.707 ± 0.025	302.3 ± 1.1
w CDM ($c_{de}^2 = 1$)	1.710 ± 0.029	302.3 ± 1.1
w CDM ($c_{de}^2 = 0$)	1.711 ± 0.025	302.4 ± 1.1
Λ CDM $m_\nu > 0$	1.769 ± 0.040	306.7 ± 2.1
Λ CDM $N_{eff} \neq 3$	1.714 ± 0.025	304.4 ± 2.5
Λ CDM $\Omega_k \neq 0$	1.714 ± 0.024	302.5 ± 1.1
$w(z)$ CDM CPL ($c_{de}^2 = 1$)	1.710 ± 0.026	302.5 ± 1.1
Λ CDM + tensor	1.670 ± 0.036	302.0 ± 1.2
Λ CDM + running	1.742 ± 0.032	302.8 ± 1.1
Λ CDM + running + tensor	1.708 ± 0.039	302.8 ± 1.2
Λ CDM + features	1.708 ± 0.028	302.2 ± 1.1

TABLE I: The 68% C.L. limits on the shift parameter R and the acoustic scale derived from the WMAP data. A top-hat age prior $10 \text{ Gyrs} < t_0 < 20 \text{ Gyrs}$ is assumed.

spectrum due to a sharp step in the inflaton potential as in [37].

As we can see from Table I the constraints on R and l_a are stable under minimal modifications of the dark energy model parameters, differences are smaller than few per cent including the case of a clustered dark energy component ($c_{de}^2 = 0$). In contrast the confidence interval of l_a is shifted by few per cent in the Λ CDM model with the neutrino mass or an extra background of relativistic particles, while the values of R are slightly modified for a running of the primordial power spectrum or the contribution of tensor modes. These results confirm previous analysis [11, 12].

Although the values of R and l_a are nearly the same for the dark energy models we have considered, this should not be considered as an incentive to use these parameters without caution. For instance there is no specific reason as to why one should use the values of R and l_a inferred from the vanilla Λ CDM, rather than those obtained accounting for the neutrino mass. Consequently one may infer slightly different bounds on the dark energy parameters depending whether neutrinos are assumed to be massless or not. Moreover the fact that WMAP data constrain R and l_a to be nearly the same for simple dark energy models is because the effect of dark energy on the epoch of matter-radiation equality and the evolution of the density perturbations remains marginal. This might not be the case for other models, such as those for which the dark energy density is a non-negligible at early times. Since this effect is not accounted for in the values of R and l_a inferred from the vanilla Λ CDM, their use may lead to strongly biased results. In contrast the location of the CMB extrema is applicable to this class of models as well [17]. A similar consideration applies to inhomogeneous models in which the late times dynamics and geometry departs from that of the standard FRW universe [38].

The applicability to models of modified gravity, such as the DGP scenario [39] deserves a separate comment. In these models not only the Hubble law differs from the standard Λ CDM, but also the evolution of the density perturbations can be significantly different. Therefore

unless the evolution of the linear perturbations is understood well enough as to allow for a precise calculation of the CMB and matter power spectra, the use R and l_a , or alternatively of the position of the CMB extrema or the distance measurements from BAO might expose to the risk of completely wrong results.

VI. CONCLUSIONS

The multipoles of the CMB extrema can be directly measured from the WMAP spectra and used to combine CMB information with other cosmological datasets. Corrections to the location of the CMB peaks and dips from pre-recombination effects need to be taken into account for an unbiased parameter inference. Here we have shown that the position of the first peak as measured by WMAP-3yrs data is strongly displaced with the respect to the actual location of the acoustic horizon at recombination. This displacement is caused by gravitational driving forces affecting the propagation of sound waves before recombination. These effects are smaller on higher harmonics, indicating the presence of a scale dependent phase shift which becomes negligible on scales well inside the horizon.

We have performed a cosmological parameter inference using the position of the WMAP peaks and dips in combination with recent BAO measurements and derived constraints on a constant dark energy equation of state under different model parameter assumptions.

The method we have presented here is alternative to using the shift parameter R and/or the multipole of the

acoustic horizon at decoupling l_a . We have tested for potential model dependencies of R and l_a by running a full CMB spectra likelihood analysis for different class of models. Indeed for simple dark energy models the inferred constraints on R and l_a do not differ from those inferred assuming the vanilla Λ CDM. Nevertheless we have suggested caution in using these secondary parameters as *data*, since hidden assumptions may lead to biased results particularly when testing models which greatly depart from the Λ CDM cosmology.

Indeed we do advocate the use of the full CMB spectra, particularly for constraining the properties of dark energy. In fact more information on dark energy is encoded in the full CMB spectrum than just in the distance to the last scattering surface. Nevertheless we think that using the location of the CMB extrema provide a self-consistent approach for combining in a friendly user way the CMB information with complementary cosmological data.

Acknowledgments

PSC is grateful to the Aspen Center for Physics for the hospitality during the “Supernovae as Cosmological Distance Indicators” Workshop where part of this work has been developed. We are particularly thankful to Jean-Michel Alimi, Laura Covi, Michael Doran, Malcom Fairbairn, Jan Hamann, Martin Kunz, Julien Larena, Eric Linder, Yun Wang and Martin White for discussions, suggestions and help. We acknowledge the use of CosmoMC [40] for the analysis of the MCMC chains.

-
- [1] P. De Bernardis et al., *Nature*, **404**, 955 (2000); N.W. Halverson et al., *Astrophys. J.*, **568**, 38 (2002)
 - [2] M.C. Runyan et al., *New Astron. Rev.*, **47**, 915 (2003); C.L. Bennett et al., *Astrophys. J. Supp.*, **148**, 1 (2003)
 - [3] G. Hinshaw et al., *Astrophys. J. Supp.*, **170**, 288 (2007)
 - [4] A.D. Sakharov, *JETP*, **49**, 345 (1965); J. Silk, *Astrophys. J.*, **151**, 459 (1968); P.J.E. Peebles and I.T. Yu, *Astrophys. J.*, **162**, 815
 - [5] N. Vittorio and J. Silk, *Astrophys. J. Lett.*, **285**, 39 (1984); J.R. Bond and G. Efstathiou, *Astrophys. J. Lett.*, **285**, 45 (1984); A.G. Doroshkevich, *Sov. Astron. Lett.*, **14**, 125 (1988)
 - [6] W. Hu and N. Sugiyama, *Phys. Rev. D***51**, 6 (1995);
 - [7] W. Hu and M. White, *Astrophys. J.*, **471**, 30 (1996)
 - [8] M. Kamionkowski, D.N. Spergel and N. Sugiyama, *Astrophys. J. Lett.*, **426**, 57 (1994)
 - [9] D.N. Spergel et al., *Astrophys. J. Supp.*, **170**, 377 (2007)
 - [10] D.J. Eisenstein, W. Hu and M. Tegmark, *Astrophys. J. Lett.*, **504**, 57 (1998)
 - [11] O. Elgaroy and T. Multamaki, *Astron. & Astrophys.*, **471**, 65 (2007)
 - [12] Y. Wang and P. Mukherjee, *astro-ph/0703780*
 - [13] W. J. Percival et al., *arXiv:0705.3323*
 - [14] W. Hu and N. Sugiyama, *Astrophys. J.*, **444**, 489 (1995)
 - [15] M.J. Rees and D.W. Sciama, *Nature*, **217**, 511 (1968)
 - [16] W. Hu, M. Fukugita, M. Zaldarriaga and M. Tegmark, *Astrophys. J.*, **549**, 669 (2001)
 - [17] M. Doran and M. Lilley, *Mont. Not. Roy. Astron. Soc.*, **330**, 965 (2002)
 - [18] L. Page et al., *Astrophys. J. Supp.*, **148**, 233 (2003)
 - [19] R. Keskitalo et al., *J. Cosmol. Astropart. Phys.*, **09**, 008 (2007)
 - [20] J. Magueijo et al., *Phys. Rev. Lett.*, **76**, 15 (1996)
 - [21] U. Seljak and M. Zaldarriaga, *Astrophys. J.*, **469**, 437 (1996); A. Lewis, A. Challinor and A. Lasenby, *Astrophys. J.* **538**, 473 (2000); M. Doran, *J. Cosmol. Astropart. Phys.*, **10**, 011 (2005)
 - [22] W. Hu and N. Sugiyama, *Astrophys. J.*, **471**, 542 (1996)
 - [23] P.S. Corasaniti and E. J. Copeland, *Phys. Rev. D***65**, 043004 (2002)
 - [24] M. Doran, M. Lilley and C. Wetterich, *Phys. Lett. B***528**, 175 (2002)
 - [25] S. Sen and A.A. Sen, *Astrophys. J.*, **588**, 1 (2003)
 - [26] M. Chevallier and D. Polarski, *Int. J. Mod. Phys. D***10**, 213 (2001)
 - [27] E. V. Linder, *Phys. Rev. Lett.* **90**, 091301 (2003)
 - [28] W. L. Freedman et al., *Astrophys. J.*, **553**, 47 (2001)
 - [29] P. Hunt and S. Sarkar, *arXiv:0706.2443*

- [30] R.R. Caldwell, M. Kamionkowski, N.N. Weinberg, Phys. Rev. Lett. 91, 071301 (2003)
- [31] S. Das, P.S. Corasaniti and J. Khoury, Phys. Rev. D**73**, 083509 (2006)
- [32] G.-B. Zhao et al., Phys. Lett. B**648**, 8 (2007)
- [33] J.R. Bond, G. Efstathiou and M. Tegmark, Mont. Not. Roy. Astron. Soc., 291, L33 (1997)
- [34] R. Bowen, S.H. Hansen, A. Melchiorri, J. Silk and R. Trotta, Mon. Not. Roy. Astron. Soc., 334, 760 (2002); S. H. Hansen et al., Phys. Rev. D**65** 023511 (2002)
- [35] G.L. Fogli et al., Phys. Rev. D**75**, 053001 (2007); G. L. Fogli et al., Phys. Rev. D**70** 113003 (2004)
- [36] W. H. Kinney, E. W. Kolb, A. Melchiorri and A. Riotto, Phys. Rev. D**74** 023502 (2006)
- [37] L. Covi, J. Hamann, A. Melchiorri, A. Slosar and I. Sorbera, Phys. Rev. D**74** 083509 (2006); J. Hamann, L. Covi, A. Melchiorri and A. Slosar, Phys. Rev. D**76** 023503 (2007)
- [38] J. Larena et al., in preparation
- [39] G.R. Dvali, G. Gabadadze and M. Porrati, Phys. Lett. B**485**, 208 (2000); C. Deffayet, Phys. Lett. B**502**, 199 (2001)
- [40] A. Lewis and S. Bridle, Phys. Rev. D**66**, 103511 (2002)